C. R. Mecanique 342 (2014) 198–207

Contents lists available at ScienceDirect

Comptes Rendus Mecanique

www.sciencedirect.com

Micromechanics of granular materials – A tribute to Ching S. Chang

Microstructural formulation of stress dilatancy

Formulation microstructurelle de la dilatance

Richard Wan [a,*], Peijun Guo [b]

[a] *Department of Civil Engineering, University of Calgary, Calgary, Alberta, T2N 1N4, Canada*
[b] *Department of Civil Engineering, McMaster University, Hamilton, Ontario, L8S 4L7, Canada*

ARTICLE INFO

Article history:
Available online 28 February 2014

Keywords:
Stress-dilatancy
Fabric
Elastoplasticity
Micromechanics

Mots-clés :
Dilatance
Texture
Élastoplasticité
Micromécanique

ABSTRACT

In this work, we show that the well-known Rowe's stress-dilatancy relation can be readily recovered from a micromechanical analysis of an assembly of rigid particles as a purely dissipative system in the case of a regular packing. When the analysis is extended to a random packing, one can explicitly incorporate the dependence of fabric, density and stress level on dilatancy, a basic aspect of geomaterial behaviour. The resulting microstructurally based stress dilatancy relation can be easily implemented as a non-associated flow rule in any standard elastoplastic model. Some numerical simulations of stress-dilatancy with initial fabric as a controlling variable are presented to illustrate the developed model.

RÉSUMÉ

On démontre dans cet article la loi de dilatance de Rowe à partir d'une analyse micromécanique sur un assemblage régulier de particules rigides purement dissipatif. Dans le cas d'un assemblage aléatoire de particules, on peut faire apparaître dans l'écriture de la dilatance l'effet de la texture, de la densité et du niveau de contrainte, une caractéristique importante des géomatériaux. La loi de dilatance issue d'une analyse micromécanique entre dans un modèle élastoplastique par l'intermédiaire d'une règle d'écoulement plastique non associée. Les différents aspects du modèle sont illustrés sur plusieurs exemples démontrant l'effet de la texture initiale sur la dilatance.

1. Introduction

The shear strength of non-cohesive granular soils is strongly influenced by the phenomenon of dilatancy first revealed by Reynolds [1] far back in 1885, and later framed within the stress-dilatancy theory worked out by Rowe [2]. However, the term dilatancy is usually loosely defined as shear induced volumetric expansion without any due reference to its micromechanical origin. In fact, upon shearing, any ensuing volumetric expansion arises from geometrical constraints imposed by the grain rearrangement against applied stresses, even in the absence of interparticle friction, see for instance [3].

* Corresponding author.
E-mail addresses: wan@ucalgary.ca (R. Wan), guop@mcmaster.ca (P. Guo).

http://dx.doi.org/10.1016/j.crme.2014.01.005
1631-0721/

Because of the intrinsic coupling between particle arrangement and volume change through important micro-kinematics such as relative sliding and rolling of particles, dilatancy and fabric are intimately linked, and as such, control material strength. This important theoretical issue has led to the systematic effort of working out continuum plasticity formulations derived from micromechanics in order to incorporate some level of particulate microstructure. There are several papers in the literature following this line of study. Among these, we recall C.S. Chang's numerous important contributions to the micromechanical analysis of granular materials, including homogenization approaches, through a series of publications such as among others: [4–6]. In the case of plasticity of granular materials, we recall the work by Chang and Hicher [7] in which the authors develop a plasticity model with embedded microstructural information. Their technique uses phenomenological plasticity to describe the complex interacting mechanisms such as rotation and sliding at the particle level, and thereafter upscale the analysis to the continuum level through homogenization.

The present work adopts an alternative approach based on a micromechanical representation of stress-dilatancy in an ensemble of rigid particles. The micromechanically developed stress-dilatancy relation then enters any standard elastoplasticity model as a flow rule. One merit of this approach is that the formulation naturally gives rise to non-associative plastic yield and flow, as well as plastic strain softening material properties that are intrinsically a function of microstructure.

To set the stage, we show that a simple micromechanical model based on an assembly of rigid particles as a purely dissipative material leads to the well-known Rowe's stress-dilatancy relation for the case of a regular assembly. When the formulation is extended to a random packing, one can explicitly incorporate one of the basic properties of geomaterials, i.e. the dependence of dilatancy on fabric, density and stress levels.

2. Microstructural analysis of stress dilatancy

We herein briefly recall the stress-dilatancy theory as a prelude to subsequent developments. In soil mechanics, the dilatancy behaviour of granular soils is usually described within Rowe's stress-dilatancy theory (Rowe, [2]). By minimizing the ratio of the rate of work done on an assembly of particles by the major principal stress to the rate of work done by the minor principal stress, Rowe arrived at his celebrated dilatancy equation, i.e.

$$\frac{\sigma_1}{\sigma_3} = K D; \quad K = \tan^2\left(45^\circ + \varphi_\mu\right); \quad D = 1 - \frac{\mathrm{d}\varepsilon_v^{\mathrm{p}}}{\mathrm{d}\varepsilon_1^{\mathrm{p}}} \tag{1}$$

where $\varphi_\mu =$ interparticle friction angle, $\mathrm{d}\varepsilon_v^{\mathrm{p}} =$ increment of plastic volumetric strain, $\mathrm{d}\varepsilon_1^{\mathrm{p}} =$ increment of axial plastic strain, whereas σ_1 and σ_3 are applied major and minor principal stresses respectively. Eq. (1) indicates that the dilatancy term D is simply a linear function of the applied stress ratio through the interparticle friction angle. However, in comparison with experimental observations, it is clear that dilatancy is also a function of fabric, density of packing and stress level during loading history. These dependencies vitiate the predictive capability of Rowe's' stress-dilatancy model Eq. (1). As such, there have been since many works on stress-dilatancy towards addressing the above-mentioned shortcomings, among many others, see [8–10].

As for dealing with fabric changes during the dilatant phase of sand deformation, Dafalias and Manzari [11] used a bounding surface plasticity framework with the plastic modulus degrading with fabric. Other approaches which are still macroscopic in nature focus on capturing detailed particle mechanics such as the double sliding model [12]. Since fabric operates directly on the way dilatancy is manifested during loading history until material failure, Wan and Guo [13–15], and Guo and Wan [16] follow a procedure in which fabric is explicitly embedded into a stress-dilatancy relationship via micromechanical analysis. It is this latter approach that will be presented here from both a micromechanical and physical vantage point. Hence, the starting point is the identification of micro- and macro-variables followed by the writing of the conservation of energy at both scales. As such, a stress dilatancy relationship involving microstructural variables such as fabric can be derived.

3. Preliminaries — micro–macro relationships

Consider a REV of volume V containing an assembly of rigid particles represented by a network of branch vectors $\boldsymbol{\ell}$ linking centres of two contacting particles. While the connectivity of particles is represented by a so-called graph of branch vectors that describes the granular structure of the REV, it is also essential to describe the relationship between local (micro) and global (macro) variables by using a homogenization or an averaging technique.

As such, following the above-mentioned procedure, we can easily derive, for N contacts in the given REV, the well-known relation between Cauchy stress ($\boldsymbol{\sigma}$) and contact force ($\mathbf{f}$), as originally introduced by Love [17], i.e.

$$\boldsymbol{\sigma} = \frac{1}{V}\sum^{N} \mathbf{f} \otimes \boldsymbol{\ell} \tag{2}$$

The inverse relationship can be obtained by a linear projection rule where the local variable is extracted as a projection of the global field along the branch vector characterizing the contact between two particles [18], i.e.

$$\mathbf{f} = \boldsymbol{\sigma} \cdot \mathbf{F}^{-1} \cdot \boldsymbol{\ell}; \quad \mathbf{F} = \frac{1}{V}\sum^{N} \boldsymbol{\ell} \otimes \boldsymbol{\ell} \tag{3}$$

where $\mathbf{F}$ is a second order tensor that describes the distribution of branch vectors, a characteristic of the granular structure of the medium, i.e. its fabric.

Defining a nominal stress $\boldsymbol{\sigma}^* = \boldsymbol{\sigma} \cdot \mathbf{F}^{-1}$ (Cauchy stress factored with fabric), we anticipate that the contact force vector $\mathbf{f}$ between two particles can be obtained as a projection of the nominal stress along the local branch vector $\boldsymbol{\ell}$ as conveyed in Eq. (3). Here, the nominal stress $\boldsymbol{\sigma}^*$ can be interpreted as a global measure of internal forces between particles together with a representation of their interconnectivity.

Similarly, considering the conservation of energy at both scales and following a minimization of the error due to the linear projection assumption [18,6], strains ($\boldsymbol{\varepsilon}$) can be determined from local variables such as relative displacements ($\Delta\mathbf{u}$), i.e.

$$\Delta\mathbf{u} = \boldsymbol{\varepsilon} \cdot \boldsymbol{\ell} \quad \text{or} \quad \boldsymbol{\varepsilon} = \frac{1}{V}\sum^{N} \Delta\mathbf{u} \cdot \mathbf{F}^{-1} \cdot \boldsymbol{\ell} \tag{4}$$

We note that the kinematic localization in Eq. (4) refers to an affine projection that may be restrictive, especially when the meso-structure intervenes. Having established the link between macro- and micro-statical variables, we now examine sliding at the particle contact scale where tangential (f_t) and normal forces (f_n) act against interparticle friction angle φ_μ. Relative sliding will be initiated as soon as the tangential contact force f_t reaches its limiting value, i.e. when $f_\mathrm{t} = f_\mathrm{n} \tan\varphi_\mu$.

In general, for a given contact of orientation $\mathbf{n}$, the tangential and normal contact forces can be defined as:

$$f_\mathrm{n} = \mathbf{f} \cdot \mathbf{n}; \qquad f_\mathrm{t} = \mathbf{f} \cdot \mathbf{t}; \qquad \mathbf{f} = \boldsymbol{\sigma} \cdot \mathbf{F}^{-1} \cdot \boldsymbol{\ell} \tag{5}$$

where the unit vector $\mathbf{t}$ is contained in the plane of contact such that:

$$\mathbf{t} \cdot \mathbf{n} = 0; \qquad \mathbf{t} \cdot \mathbf{t} = 1; \qquad \mathbf{n} \cdot \mathbf{n} = 1 \tag{6}$$

As such, the direction of local sliding contained in the tangential plane follows as:

$$\frac{f_\mathrm{t}}{f_\mathrm{n}} = \frac{\mathbf{f} \cdot \mathbf{t}}{\mathbf{f} \cdot \mathbf{n}} = \tan\varphi_\mu \Rightarrow \mathbf{f} \cdot (\mathbf{t} - \mu\mathbf{n}) = 0 \tag{7}$$

where $\mu = \tan\varphi_\mu$ is the coefficient of friction between two particles. If we express the vector $\mathbf{f}$ as a linear combination of directions $\mathbf{n}$ and $\mathbf{t}$, and applying the orthogonality condition in Eq. (7), we obtain:

$$\mathbf{f} = f_\mathrm{n}(\mu\mathbf{t} + \mathbf{n}); \quad f_\mathrm{n} = \|\mathbf{f}\| \cos\varphi_\mu \tag{8}$$

4. Stress-dilatancy through a purely dissipative formulation

The essential idea is to express the energies at the two scales in order to eventually recover an analytical expression that describes stress-dilatancy in terms of microstructural parameters. More precisely, the work input to deform the material within an increment of strain is transferred down to the particle level, and noting Eqs. (3) and (4), we get:

$$\boldsymbol{\sigma} \cdot \dot{\boldsymbol{\varepsilon}} = \frac{1}{V}\sum^{N} \mathbf{f} \cdot \Delta\dot{\mathbf{u}} = \frac{1}{V}\sum^{N} \left(\boldsymbol{\sigma} \cdot \mathbf{F}^{-1} \cdot \boldsymbol{\ell}\right) \cdot (\dot{\boldsymbol{\varepsilon}} \cdot \boldsymbol{\ell}) \tag{9}$$

If a distinction is made between the number of contacts that slide (N_s) and those which remain intact ($N_{\bar{\mathrm{s}}}$), and noting Eq. (8), Eq. (9) can be re-written as:

$$\boldsymbol{\sigma} \cdot \dot{\boldsymbol{\varepsilon}} = \left(\bar{\mathbf{F}} + \boldsymbol{\sigma} \cdot \mathbf{F}^{-1} \cdot \bar{\bar{\mathbf{F}}}\right) \cdot \dot{\boldsymbol{\varepsilon}} \tag{10}$$

with

$$\bar{\mathbf{F}} = \frac{1}{V}\sum^{N_\mathrm{s}} \left[f_\mathrm{n}(\mu\mathbf{t} + \mathbf{n})\right] \otimes \boldsymbol{\ell} \quad \text{and} \quad \bar{\bar{\mathbf{F}}} = \frac{1}{V}\sum^{N_{\bar{\mathrm{s}}}} \boldsymbol{\ell} \otimes \boldsymbol{\ell} \tag{11}$$

The tensor $\bar{\mathbf{F}}$ represents a stress quantity that arises from particle contacts which slide according to a certain statistical distribution. On the other hand, the tensor $\bar{\bar{\mathbf{F}}}$ refers to the fabric tensor, except that it is calculated based on the network of contacts that do not slide. Therefore, we can ideally define two networks of particle connectivity, namely a strong and a weak one [19] that would develop during deformation history. Any force chains showing magnitudes of above- and below-average forces would constitute a strong and weak network respectively.

5. Two-dimensional case

Without any loss in generality, we consider a simple 2-D example in which Eq. (10) indeed reduces to Rowe's stress-dilatancy [2]. Consider a REV subjected to a biaxial state of stress (σ_1, σ_2) as illustrated in Fig. 1. During the course of loading, some particles will slide, while others will remain intact. When a plastic limit state is reached, a saw-tooth failure surface AB develops which can be smoothened into a mean plane in which sliding occurs along the resultant of all local slip directions occurring at particle contacts. The energy dissipated in the REV at failure is thus equal to the sum of all local frictional dissipation occurring between particles on the failure surface.

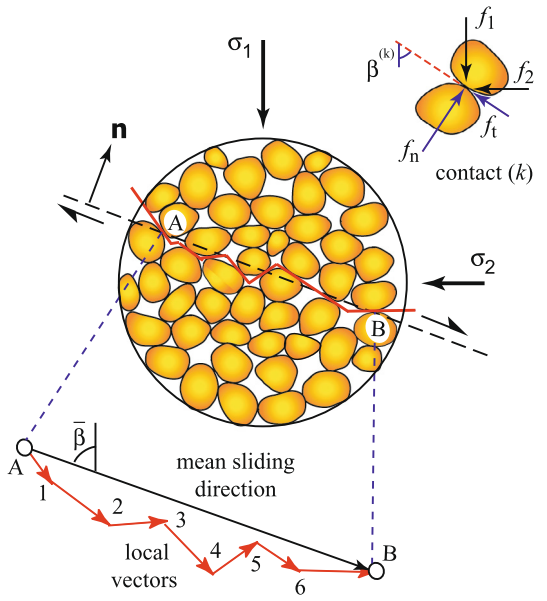

Fig. 1. (Color online.) Notion of failure surface: local and global sliding in a REV.

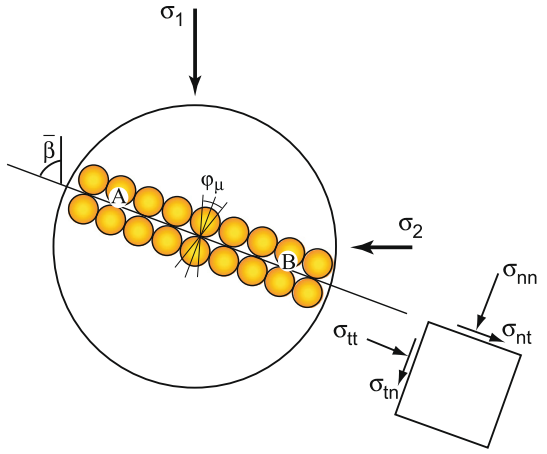

Fig. 2. (Color online.) Failure surface in the case of a regular packing.

5.1. Case of a regular assembly of particles

Upon further expanding Eq. (10), we arrive at three terms:

$$\boldsymbol{\sigma}\cdot\dot{\boldsymbol{\varepsilon}}=\frac{1}{V}\sum^{N_s}\mu f_n\mathbf{t}\cdot\dot{\boldsymbol{\varepsilon}}\cdot\boldsymbol{\ell}+\frac{1}{V}\sum^{N_s}f_n\mathbf{n}\cdot\dot{\boldsymbol{\varepsilon}}\cdot\boldsymbol{\ell}+\frac{1}{V}\sum^{N_{\bar{s}}}\left(\boldsymbol{\sigma}\cdot\mathbf{F}^{-1}\cdot\boldsymbol{\ell}\right)\cdot\left(\dot{\boldsymbol{\varepsilon}}\cdot\boldsymbol{\ell}\right) \tag{12}$$

When the plastic limit state is reached, the first term of the right-hand side of Eq. (12) pertains to the energy dissipated at sliding contacts that concentrate mainly along the failure surface AB. The second term refers to the work done by contact forces normal to AB, while the last term arises from the homogenization process and relates to the work done by non-sliding contacts outside AB. Before examining the case of a random microstructure, let us consider a regular packing in which the global failure surface coincides with the local interparticle sliding directions, see Fig. 2.

As such, by choosing an elementary volume adjacent to the failure surface AB with stresses acting on each face of the element, each term in Eq. (12) can be written explicitly as:

$$\frac{1}{V}\sum^{N_s}\mu f_n\mathbf{t}\cdot\dot{\boldsymbol{\varepsilon}}\cdot\boldsymbol{\ell}=\frac{1}{V}\sum^{N_s}f_t\Delta\dot{u}_t\equiv\sigma_{tn}\dot{\varepsilon}_{tn}$$

$$\frac{1}{V}\sum^{N_s}f_n\mathbf{n}\cdot\dot{\boldsymbol{\varepsilon}}\cdot\boldsymbol{\ell}=\frac{1}{V}\sum^{N_s}f_n\Delta\dot{u}_n\equiv\sigma_{nn}\dot{\varepsilon}_{nn}$$

$$\frac{1}{V}\sum^{N_{\bar{s}}}\left(\boldsymbol{\sigma}\cdot\mathbf{F}^{-1}\cdot\boldsymbol{\ell}\right)\cdot\left(\dot{\boldsymbol{\varepsilon}}\cdot\boldsymbol{\ell}\right)=(\boldsymbol{\sigma}\cdot\dot{\boldsymbol{\varepsilon}})_{\text{internal}}\equiv\sigma_{\text{tt}}\dot{\varepsilon}_{\text{tt}} \tag{13}$$

Herein, the plastic dissipation is restricted to the sliding plane AB, where only relative tangential displacement ($\Delta\dot{u}_{\text{t}}$) occurs, while the associated normal component is zero. Thus,

$$\begin{aligned}\boldsymbol{\sigma}\cdot\dot{\boldsymbol{\varepsilon}}&=\sigma_{\text{tt}}\dot{\varepsilon}_{\text{tt}}+\sigma_{\text{tn}}\dot{\varepsilon}_{\text{tn}}\\&=\left(\frac{\sigma_1+\sigma_2}{2}+\frac{\sigma_1-\sigma_2}{2}\sin\varphi_\mu\right)\left(\frac{\dot{\varepsilon}_1+\dot{\varepsilon}_2}{2}+\frac{\dot{\varepsilon}_1-\dot{\varepsilon}_2}{2}\sin\varphi_\mu\right)\\&\quad+\left(\frac{\sigma_1-\sigma_2}{2}\cos\varphi_\mu\right)\left(\frac{\dot{\varepsilon}_1-\dot{\varepsilon}_2}{2}\cos\varphi_\mu\right)\end{aligned} \tag{14}$$

since the operative friction angle on plane AB is equal to φ_μ. Generally speaking, this friction angle should be denoted as φ_{f} which is a characteristic of the local particle arrangement and does not coincide with φ_μ. This will be demonstrated analytically through micromechanical calculations in later sections of this paper.

Finally, noting $\boldsymbol{\sigma}\cdot\dot{\boldsymbol{\varepsilon}}=\sigma_1\dot{\varepsilon}_1+\sigma_2\dot{\varepsilon}_2$, and advocating the Mohr–Coulomb failure criterion together with the introduction of a dilatancy angle ψ such that $\sin\psi=-(\dot{\varepsilon}_1+\dot{\varepsilon}_2)/(\dot{\varepsilon}_1-\dot{\varepsilon}_2)$, we finally obtain the well-known Rowe's stress-dilatancy relation in 2-D:

$$\sin\psi=-\frac{(\dot{\varepsilon}_1/\dot{\varepsilon}_2+1)}{(\dot{\varepsilon}_1/\dot{\varepsilon}_2-1)}=\frac{\sin\varphi_{\text{m}}-\sin\varphi_\mu}{1-\sin\varphi_{\text{m}}\sin\varphi_\mu} \tag{15}$$

where the mobilized friction φ_{m} is determined from $\sin\varphi_{\text{m}}=(\sigma_1-\sigma_2)/(\sigma_1+\sigma_2)$.

It is interesting to note that Rowe [2] had originally pointed out that the friction angle φ_μ appearing in Eq. (15) refers to a dense packing and should be replaced with φ_{cv}, the friction angle at critical state, for a loose packing. By extension to an arbitrary particle packing, we can intuitively replace φ_μ in Eq. (15) with the characteristic friction angle φ_{f}. This will be formally demonstrated next.

5.2. Case of a random particle packing

Let us consider the case of a random particle assembly for which the failure plane develops along the mean direction $\bar{\beta}$ defined as the resultant of all local particle sliding directions, see Fig. 1. The summation of all contact forces in the failure plane gives the resultant force vector with the ratio of the normal to tangential component equal to $\tan(\varphi_{\text{f}}+\bar{\beta})$. Hence, the characteristic friction angle φ_{f} can be determined. The latter angle necessarily varies with the topology of the failure plane, the stress level, as well as the number of sliding contacting particles that eventually lose contact. If all particles were to slide along the same direction, we would recover the regular packing case for which $\varphi_{\text{f}}=\varphi_\mu$.

Consider a given contact (k) with the tangent plane oriented at an angle $\beta^{(k)}$ with the vertical. The contact will not slide as long as the ratio $\mu^{(k)}_{\text{mob}}$ of tangential over normal force remains less than $\mu=\tan\varphi_\mu$. Thus, noting Eq. (3), we get:

$$\mu^{(k)}_{\text{mob}}=\frac{f_1^{(k)}\cos\beta^{(k)}-f_2^{(k)}\sin\beta^{(k)}}{f_1^{(k)}\sin\beta^{(k)}+f_2^{(k)}\cos\beta^{(k)}}=\frac{\sigma_{11}F_{11}^{-1}l_1^{(k)}\cos\beta^{(k)}-\sigma_{22}F_{22}^{-1}l_2^{(k)}\sin\beta^{(k)}}{\sigma_{11}F_{11}^{-1}l_1^{(k)}\sin\beta^{(k)}+\sigma_{22}F_{22}^{-1}l_2^{(k)}\cos\beta^{(k)}} \tag{16}$$

If we further consider that the branch vectors are collinear with the normal to the contact plane, then $l_1^{(k)}=\sin\beta$ and $l_2^{(k)}=\cos\beta$. By defining a nominal stress $\boldsymbol{\sigma}^*=\boldsymbol{\sigma}\cdot\mathbf{F}^{-1}$ which accounts for fabric, let us introduce a nominal friction angle such that $\sin\bar{\varphi}^*_{\text{m}}=(\sigma^*_{11}-\sigma^*_{22})/(\sigma^*_{11}+\sigma^*_{22})$. Thus, reorganizing Eq. (16), we get:

$$\mu^{(k)}_{\text{mob}}=\frac{\sin\bar{\varphi}^*_{\text{m}}\sin2\beta^{(k)}}{1-\sin\bar{\varphi}^*_{\text{m}}\cos2\beta^{(k)}} \tag{17}$$

Next, we can determine all orientations $\beta^{(k)}$ of local contact planes that will potentially slide by applying the slip condition $\mu^{(k)}_{\text{mob}}>\mu$ to Eq. (17). As such, we find a range of sliding angles $\beta^{(k)}$ bounded by β_{min} and β_{max} whose values are given by:

$$\beta_{\text{min}}=\frac{1}{2}\sin^{-1}\left(\frac{\sin\varphi_\mu}{\sin\bar{\varphi}^*_{\text{m}}}\right)-\frac{\varphi_\mu}{2};\qquad\beta_{\text{max}}=\frac{\pi}{2}-\frac{1}{2}\sin^{-1}\left(\frac{\sin\varphi_\mu}{\sin\bar{\varphi}^*_{\text{m}}}\right)-\frac{\varphi_\mu}{2} \tag{18}$$

Under deviatoric loading, the nominal friction angle $\bar{\varphi}^*_{\text{m}}$ is gradually mobilized until it reaches a value φ_μ when a failure plane emerges in the direction $\beta=\pi/4-\varphi_\mu/2$, which coincides with the classic Coulomb's solution. For values of $\bar{\varphi}^*_{\text{m}}$ larger than φ_μ when more particles slide with respect to each other, the difference δ_β between β_{min} and β_{max} is reduced,

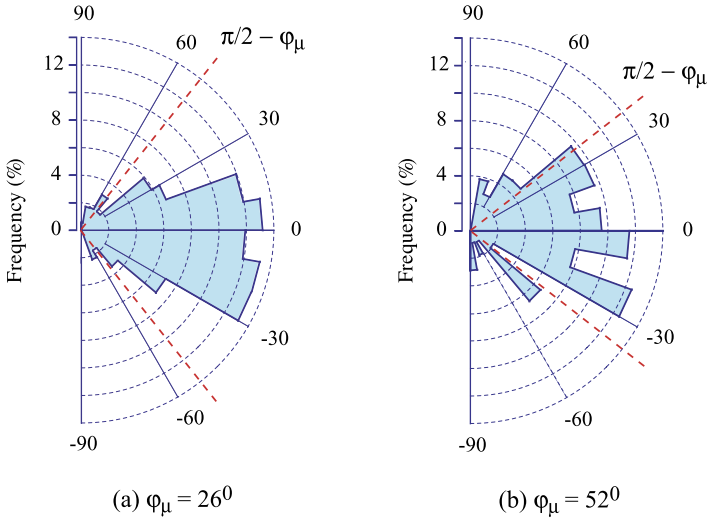

Fig. 3. (Color online.) Evolution of contacts from initial state to peak for rods of oval cross-section (data after Oda et al. [20] and Konishi et al. [21]).

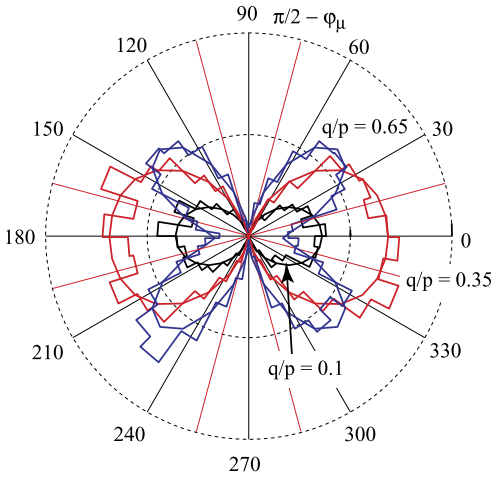

Fig. 4. (Color online.) Directional distribution of sliding contacts at various shear stresses (data after Alonso-Marroquin et al. [23]).

i.e.

$$\delta_\beta = \beta_{\max} - \beta_{\min} = \frac{\pi}{2} - \frac{1}{2}\sin^{-1}\left(\frac{\sin\varphi_\mu}{\sin\bar{\varphi}^*_{\mathrm{m}}}\right) \tag{19}$$

In fact, δ_β varies between zero (when sliding is initiated) and $(\pi/2-\varphi_\mu)$ (when $\sin\bar{\varphi}^*_{\mathrm{m}}$ reaches its maximum value of 1). There are both experimental and numerical supports for the validity of Eq. (19). For instance, Oda et al. [20] and Konishi et al. [21] observed in a series of biaxial compression tests on assemblies of oval cross-sectional rods that the evolution of contacts with relative sliding and rolling was limited over a certain range of orientations with $0 \leqslant \beta \leqslant (\pi/2-\varphi_\mu)$ as shown in Fig. 3. More experimental evidence which confirms that relative particle sliding occurs at $0 \leqslant \beta \leqslant (\pi/2-\varphi_\mu)$ can also be found in Calvetti et al. [22]. We also note that, within the framework of discrete element simulations of biaxial compression tests, the same range of sliding contact orientations as in the above is confirmed.

Fig. 4 shows the directional distribution of the sliding contacts at different shear stress levels (Alonso-Marroquin et al. [23]) where the range of sliding contact orientation increases with shearing and $\beta_{\max}$ gradually approaches $(\pi/2-\varphi_\mu)$.

In keeping with Eq. (19), it is convenient to consider a mean direction for sliding defined as:

$$\bar{\beta} = \frac{1}{2}(\beta_{\max} + \beta_{\min}) = \frac{\pi}{4} - \frac{\varphi_\mu}{2} \tag{20}$$

to define the macroscopic failure plane. On such a plane oriented at an angle $\bar{\beta}$ with the major principal stress direction, we can systematically define a nominal or characteristic friction angle φ_{f} by integrating local slips along all contact planes

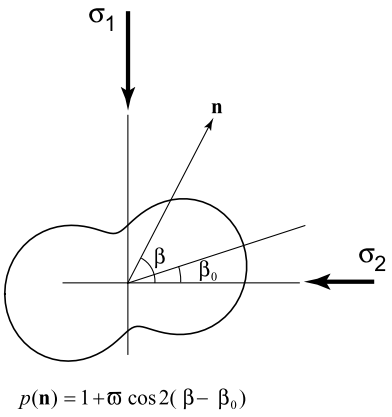

Fig. 5. Distribution of contacts with respect to principal stress directions.

contained between orientations $\beta_{\min}$ and $\beta_{\max}$. In particular, we consider a distribution of contact normals ($\mathbf{n}$) with a classic probability density function $p(\mathbf{n})$ (Rothenburg and Bathurst [24]) from a Fourier series, i.e.

$$p(\mathbf{n}) = 1 + \varpi \cos 2(\beta - \beta_0) \tag{21}$$

where β is the angle that the contact plane between two particles makes with the major principal stress direction, see Fig. 5. The direction of major contacts normals is given by β_0, while the parameter ϖ represents the degree of anisotropy of the particle packing.

By applying the distribution represented in Eq. (21) to all contacts satisfying the slip condition $(f_1^{(k)}/f_2^{(k)}) = \tan(\varphi_\mu + \beta^{(k)})$, and integrating between $\beta_{\min}$ and $\beta_{\max}$, we get:

$$\begin{aligned}\mu_{\mathrm{f}} = \tan\varphi_{\mathrm{f}} &\simeq \frac{1}{\delta_\beta}\int_{-\delta_\beta/2}^{\delta_\beta/2} \tan(\varphi_\mu + \beta)\big[1 + \varpi\cos 2(\beta - \beta_0)\big]\,\mathrm{d}\beta \\ &= \frac{1}{\delta_\beta}\ln\frac{\cos(\varphi_\mu - \delta_\beta/2)}{\cos(\varphi_\mu + \delta_\beta/2)} + \frac{\varpi}{6}\left[\tan\left(\varphi_\mu + \frac{\delta_\beta}{2}\right)\cos(\delta_\beta - 2\beta_0)\right. \\ &\quad \left. + \tan\left(\varphi_\mu - \frac{\delta_\beta}{2}\right)\cos(\delta_\beta + 2\beta_0) + 4\tan\varphi_\mu\cos 2\beta_0\right]\end{aligned} \tag{22}$$

It is noted that the friction angle φ_{f} reaches its minimum and maximum value when $\delta_\beta = 0$ and $\delta_\beta = \pi/2 - \varphi_\mu$ respectively, i.e.

$$\tan\varphi_{\mathrm{fmin}} = \lim_{\delta_\beta \to 0}\tan\varphi_{\mathrm{f}} \simeq (1 + \varpi\cos 2\beta_0)\tan\varphi_\mu \tag{23}$$

$$\tan\varphi_{\mathrm{fmax}} \simeq \frac{1}{\frac{\pi}{2} - \varphi_\mu}\ln\frac{\cos(\frac{\pi}{4} - \frac{3\varphi_\mu}{2})}{\cos(\frac{\pi}{4} + \frac{\varphi_\mu}{2})} + \frac{\xi\sin 2\beta_0 + 2(\xi\sin\varphi_\mu + 1)\tan\varphi_\mu\cos 2\beta_0}{3}\varpi \tag{24}$$

where $\xi = \cos^2\varphi_\mu/(\sin\varphi_\mu + \cos 2\varphi_\mu)$.

We next link the anisotropy parameter ϖ to the fabric tensor $\mathbf{F}$ defined by Satake [25] as:

$$F_{ij} = \frac{1}{2\pi}\int_0^{2\pi} p(\mathbf{n}) n_i n_j\,\mathrm{d}\beta \tag{25}$$

and noting Eq. (21),

$$\frac{F_{11} - F_{22}}{F_{11} + F_{22}} = \frac{1}{2}\varpi\cos 2\beta_0; \quad F_{12} = F_{21} = \frac{1}{4}\varpi\sin 2\beta_0 \tag{26}$$

The fabric tensor is generally non-coaxial with the stress tensor. The direction of major principal fabric makes an angle of β_0 with the minor principal stress (σ_2). Hence, the components of the major fabric tensor are given as:

$$\frac{F_1 - F_2}{F_1 + F_2} = \frac{1}{2}\varpi; \quad F_1 + F_2 = 1 \tag{27}$$

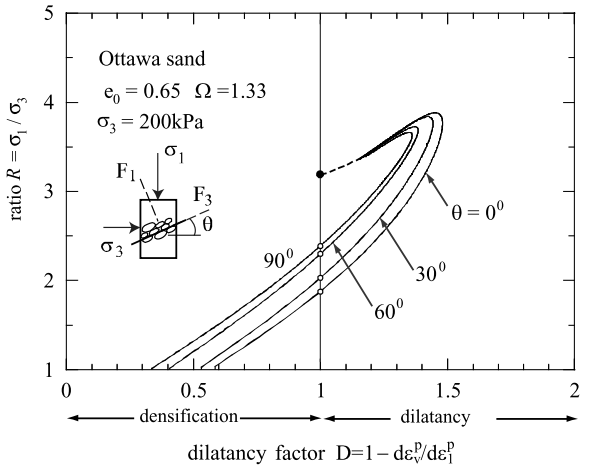

Fig. 6. Dilatancy response of sand as a function of initial fabric as computed from enriched stress-dilatancy equation.

Finally, inserting Eqs. (26), (27) into (23) and making some approximations, we get:

$$\sin\varphi_{\mathrm{f}\min} \simeq \frac{F_{22}}{F_{11}}\sin\varphi_{\mu} \tag{28}$$

In general, φ_{f} tends to its limiting value φ_{cv} when plastic deviatoric strains γ^{p} develop at the critical state. Furthermore, noticing Eq. (28) which shows a dependence on fabric, we can put forward a phenomenological evolution law for φ_{f} such as:

$$\sin\varphi_{\mathrm{f}} = \frac{XF_{22}/F_{11}+\gamma^{\mathrm{p}}}{a+\gamma^{\mathrm{p}}}\sin\varphi_{\mathrm{cv}} \tag{29}$$

where X and a are constants. We can further incorporate the influence of density (void ratio) by adding a void ratio dependent factor, i.e.

$$\sin\varphi_{\mathrm{f}} = \frac{XF_{22}/F_{11}+\gamma^{\mathrm{p}}}{a+\gamma^{\mathrm{p}}}\left(\frac{e}{e_{\mathrm{cr}}}\right)^{n_{\mathrm{f}}}\sin\varphi_{\mathrm{cv}} \tag{30}$$

where n_{f} is an exponent and e_{cr} is the void ratio at critical state.

Thus, by means of the substitution $\varphi_{\mu} \to \varphi_{\mathrm{f}}$ into Eq. (15) which far back in this contribution referred to the original Rowe's stress-dilatancy relation, Eq. (30) enriches the original stress dilatancy relation in that it now accounts for additional dependencies such as fabric (F_{22}/F_{11}), density (e), and the stress level (e_{cr} depends on the mean stress p).

Accordingly, as proposed in Wan et al. [26], it is possible to further generalize the stress-dilatancy equation to a three-dimensional case as:

$$\sin\psi_{\mathrm{m}} = \frac{\sin\varphi_{\mathrm{m}}-\sin\varphi_{\mathrm{f}}}{1-\sin\varphi_{\mathrm{m}}\sin\varphi_{\mathrm{f}}}; \qquad \sin\varphi_{\mathrm{f}} = \frac{\alpha_{\mathrm{f}}+\gamma^{\mathrm{p}}}{\alpha_0+\gamma^{\mathrm{p}}}\left(\frac{e}{e_{\mathrm{cr}}}\right)^{n_{\mathrm{f}}}\sin\varphi_{\mathrm{cv}} \tag{31}$$

where ψ_{m} is the mobilized dilatancy angle, φ_{m} is the mobilized friction angle as a function of stresses, α_0 is a constant, and the fabric dependency is provided through α_{f} given by:

$$\alpha_{\mathrm{f}} = \chi\left(\frac{1}{p}\mathbf{F}:\boldsymbol{\sigma}\right)^{-1}\sin\varphi_{\mathrm{cv}} \tag{32}$$

with χ being a proportionality constant. The relation in Eq. (31) with embedded fabric, stress and density levels enters in any standard elastoplastic model as a plasticity flow rule.

6. Stress dilatancy as a function of initial fabric

As an illustration of the capabilities of the enriched stress-dilatancy relation, some numerical simulations obtained within the framework of an elastoplastic model are herein presented. The interested reader is directed to a series of publications [8,9,13–15] in which Eq. (31) was implemented into an elastoplastic model with various degrees of complexity.

Fig. 6 depicts the computed dilatancy response of Ottawa sand starting with the same initial density and confining stress ($e_0 = 0,65, \sigma_3 = 200$ kPa), but with a different initial fabric for each triaxial compression test. The initial fabric is described by the principal fabric components (F_1 and F_3) of the fabric tensor as well as its principal directions (θ in Fig. 6). The

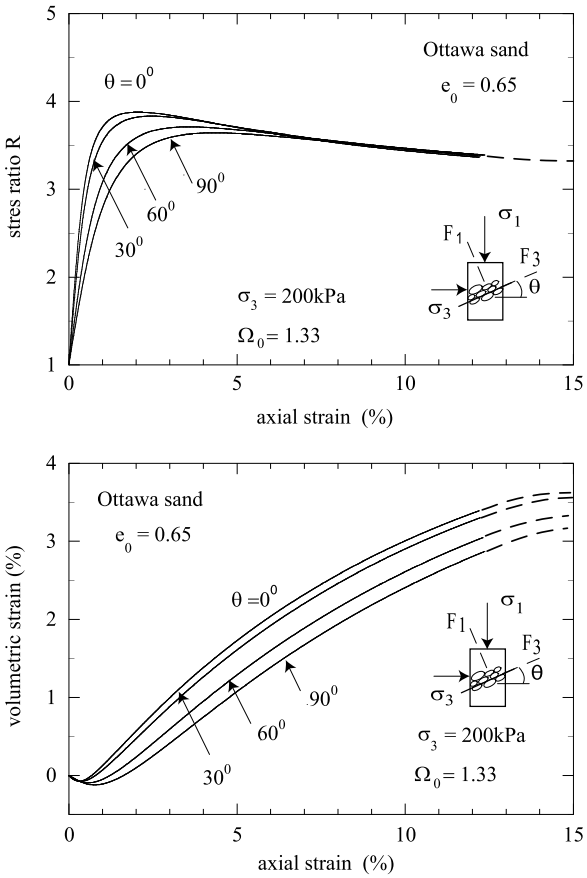

Fig. 7. Influence of initial fabric (bedding plane orientation) on the stress-volumetric response.

principal fabric ratio $\Omega = F_1/F_3$ is introduced to refer to the degree of initial anisotropy, while the angle θ corresponds to the major direction of orientations of interparticle contact planes in space. In fact, the angle θ is closely linked to the bedding angle of the particles during sample preparation. Different sample preparation methods lead to different initial fabrics, hence, justifying this study as different stress strain responses and strength characteristics of sand will be observed accordingly. Fig. 6 displays different characteristic dilatancy curves in the space as a function of. It is noted that, in contrast to the above, Rowe's equation (Eq. (1)) gives a straight line in the same space (R, D), irrespective of the initial density, confining stress and fabric. In fact this non-uniqueness in the characteristic dilatancy curve with respect to operative state variables is essential in describing the correct behaviour of sand, especially in the cyclic loading regime, as previously demonstrated in Wan and Guo [14].

In line with the various stress-dilatancy responses displayed by the model for different initial fabric, but with the same initial void ratio, the corresponding stress and volumetric strain responses are shown in Fig. 7. The influence of fabric is clearly demonstrated since a wide range of material response is obtained. For example, for a vertical bedding plane that is parallel to the direction of major principal stress, both the peak strength and shear dilation responses are subdued. In fact, a vertical bedding plane signifies that there are more contact normals oriented horizontally than in other directions, so that the specimen appears to be weaker in the vertical direction. Hence, there is a high potential for volume changes to occur.

If on the contrary, the bedding plane is set to be horizontal, i.e. most contact normals are oriented in the vertical direction, then the material appears to be overly strong with higher stiffness and higher peak strength, hence more producing volume dilation. The stress-volumetric trends shown in Fig. 7 concur well with experimental observations [27] where the bedding plane in a triaxial test on sand was varied while keeping the same initial void ratio.

7. Conclusions

The present study shows that Rowe's stress-dilatancy relation can be generalized to include the effect of fabric, stress and density levels by investigating a two-dimensional granular assembly with random packing. This is accomplished by working out rigorously the local sliding planes through principles of the micromechanics of granular media. The stress-dilatancy equation that is developed in this work enters any continuum plasticity model as a non-associated flow rule with plastic softening governed by fabric, stress and density levels. Some of the numerical simulations presented in this paper illustrate

how initial fabric influences the stress-volumetric response of sand as observed in laboratory experiments. The predictive capabilities of this enriched stress-dilatancy relation provides only part of a larger picture of the general topic of failure in granular materials involving nonlinear material behaviour and stability such as strain localization and diffuse failure. The ingredients of the model have been seen to provide mathematical sources of material instability as demonstrated in recent publications, see Wan et al. [26,28].

Acknowledgements

Funding provided by the Natural Science and Engineering Council of Canada is gratefully acknowledged.

References

[1] O. Reynolds, On the dilatancy of media composed of rigid particles in contact with experimental illustrations, Philos. Mag. 5 (20) (1885) 469–481.
[2] P.W. Rowe, The stress-dilatancy relation for static equilibrium of an assembly of particles in contact, Proc. R. Soc. Lond. Ser. A, Math. Phys. Sci. 269 (1962) 500–527.
[3] J.D. Goddard, A.K. Didwania, Computations of dilatancy and yield surfaces for assemblies of rigid frictional spheres, Q. J. Mech. Appl. Math. 51 (1) (1988) 14–43.
[4] C.S. Chang, C.L. Liao, Constitutive relation for a particulate medium with the effect of particle rotation, Int. J. Solids Struct. 26 (4) (1990) 437–453.
[5] C.S. Chang, Y. Chang, M.G. Kabir, Micromechanics modelling for stress-strain behaviour of granular soils, I: Theory, J. Geotech. Eng. 118 (2) (1992) 1959–1974.
[6] C.S. Chang, J. Gao, Second-gradient constitutive theory for granular material with random packing structure, Int. J. Solids Struct. 32 (16) (1995) 2279–2294.
[7] C.S. Chang, P.-Y. Hicher, An elastic–plastic model for granular materials with microstructural consideration, Int. J. Solids Struct. 42 (14) (2005) 4258–4277.
[8] R.G. Wan, P.J. Guo, A simple constitutive model for granular soils: Modified stress dilatancy approach, Comput. Geotech. 22 (2) (1998) 109–133.
[9] R.G. Wan, P.J. Guo, A pressure and density dependent dilatancy model for granular materials, Soil Found. 39 (6) (1999) 1–12.
[10] X.S. Li, Y.F. Dafalias, Dilatancy for cohesionless soils, Geotechnique 50 (4) (2000) 449–460.
[11] Y. Dafalias, M.T. Manzari, Simple plasticity sand model accounting for fabric change effects, J. Eng. Mech. 130 (6) (2004) 635–645.
[12] N. Balendran, S. Nemat-Nasser, Double sliding model for cyclic deformation of granular materials, including dilatancy effects, J. Mech. Phys. Solids 41 (3) (1993) 573–612.
[13] R.G. Wan, P.J. Guo, Effect of microstructure on undrained behaviour of sands, Can. Geotech. J. 38 (2001) 16–28.
[14] R.G. Wan, P.J. Guo, Drained cyclic behaviour of sand with fabric dependence, J. Eng. Mech. 127 (11) (2001) 1106–1116.
[15] R.G. Wan, P.J. Guo, Stress-dilatancy and fabric dependencies on sand behavior, J. Eng. Mech. 130 (6) (2004) 635–645.
[16] P.J. Guo, R.G. Wan, A rational approach to stress dilatancy modelling using an explicit micromechanical formulation, in: George E. Exadaktylos, Ioannis G. Vardoulakis (Eds.), Bifurcations, Instabilities and Degradations in Geomaterials, Springer, 2007, pp. 201–230.
[17] A.E.H. Love, A Treatise of Mathematical Theory of Elasticity, Cambridge University Press, Cambridge, UK, 1927.
[18] F. Emeriault, B. Cambou, Micromechanical modelling of anisotropic non-linear elasticity of granular medium, Int. J. Solids Struct. 33 (18) (1996) 2591–2609.
[19] F. Radjai, D. Wolf, M. Jean, J.-J. Moreau, Bimodal character of stress transmission in granular packing, Phys. Rev. Lett. 80 (1) (1998) 61–64.
[20] M. Oda, J. Konishi, S. Nemat-Nasser, Experimental micromechanical evaluation of strength of granular materials: effects of particle rolling, Mech. Mater. 1 (4) (1982) 269–283.
[21] J. Konishi, M. Oda, S. Nemat-Nasser, Induced anisotropy in assemblies of oval cross-sectional rods in biaxial compression, in: J.T. Jenkins, M. Satake (Eds.), Mechanics of Granular Materials: New Models and Constitutive Relations, Elsevier, Amsterdam, The Netherlands, 1983, pp. 31–39.
[22] F. Calvetti, G. Combe, J. Lanier, Experimental micromechanical analysis of a 2D granular material: relation between structure evolution and loading path, Mech. Cohes.-Frict. Mater. 2 (1997) 121–163.
[23] F. Alonso-Marroquin, H.J. Herrmann, I. Vardoulakis, Micromechanical Investigation of soil plasticity: An investigation using a discrete model of polygonal particles, in: Proc. 2nd Int. Symp. Continuous and Discontinuous Modeling of Cohesive-Frictional Materials, Stuttgart, Germany, 2004.
[24] L. Rothenburg, R.J. Bathurst, Analytical study of induced anisotropy in idealized granular materials, Geotechnique 39 (4) (1989) 601–614.
[25] M. Satake, Fabric tensors in granular materials, in: P.A. Vermeer, H.J. Luger (Eds.), Proceedings of the IUTAM Conference on Deformation and Failure of Granular Materials, Delft, The Netherlands, 31 August–3 September 1982, Balkema, Rotterdam, The Netherlands, 1982, pp. 63–68.
[26] R.G. Wan, M. Pinheiro, P.J. Guo, Elastoplastic modelling of diffuse instability response of geomaterials, Int. J. Numer. Anal. Methods Geomech. 35 (2) (2011) 140–160.
[27] M. Oda, Initial fabrics and their relations to mechanical properties of granular material, Soil Found. 12 (1) (1972) 17–36.
[28] R.G. Wan, M. Pinheiro, A. Daouadji, M. Jrad, F. Darve, Diffuse instabilities with transition to localization in loose granular materials, Int. J. Numer. Anal. Methods Geomech. 37 (10) (2012) 1292–1311.